

Figure 5. (a) Stereo view of the channel structure in the vicinity of the heme. The cross-section of the enzyme is oriented to include the main channel and region of undefined electron density ($F_o - F_c$ modeled at 3σ and shown in red), the modified heme, the Trp111-Tyr238-Met264 adduct, Arg426 adjacent to the large cleft, and the metal ion. The second funnel-shaped channel adjacent to the metal ion leads very close to the cavity created by the movement of Arg426. Some undefined electron density is visible in the $F_o - F_c$ map in this cavity. The region of the enzyme molecule that is included in (a) is indicated on the ribbon diagram of BpKatG shown at the top. The surface feature map generated by the program VOIDOO is presented in green. (b) Stereo view of the main channel leading to the heme. The

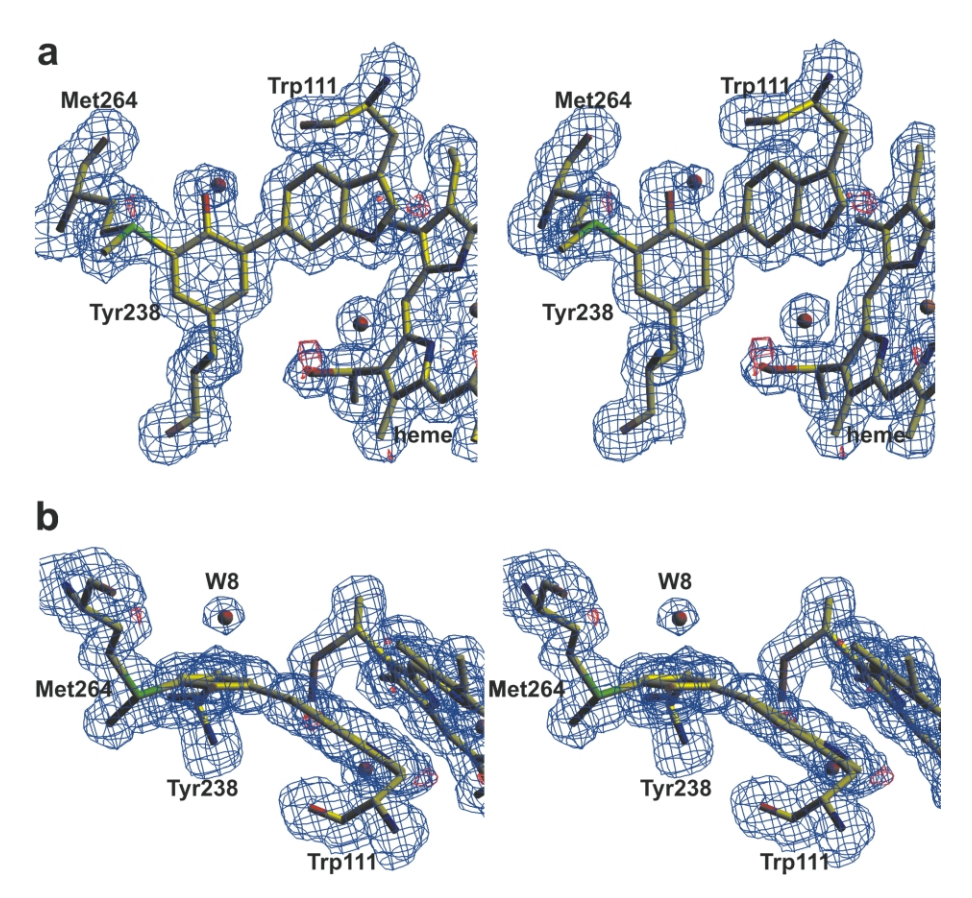


Figure 6. Two stereo views of the adduct formed among the side-chains of Trp111, Tyr238 and Met268. The $2F_{\rm o}-F_{\rm c}$ electron density map at 1σ is shown in blue and the model of the residues is superimposed. The view in (b) is rotated approximately 90° from that in (a), so that the reader is viewing the model towards the tyrosine ring OH. The intermediate sp2–sp3 nature of the bonds of the adduct on the phenyl ring of Tyr238 is evident in the deviation from planarity of the substituents on the phenyl ring in (b). The $F_{\rm o}$ - $F_{\rm c}$ electron density map at 3σ is shown in red. Note the extra density on Trp111.

as a second catalytic center besides the heme. This possibility is reinforced by the fact there is a region of undefined electron density located in the cavity vacated by the Arg426 side-chain in direct contact with the oxygen atom of the side-chain from Tyr238, the central residue of the covalent adduct.

Access channels and potential binding sites

Despite the apparent structural similarity to plant peroxidases, the larger subunit size of BpKatG (more than twice as large) results in the active site of BpKatG, including the resident heme, being buried more deeply within the subunit. The most obvious access route to the distal side of the heme, the active site of the enzyme for reaction with H₂O₂, is provided by a channel positioned similarly to, but longer than, the access route in peroxidases. The channel in BpKatG has a pronounced funnel shape and is narrowest near residues Ser324 and Asp141, about 14 Å from the

heme iron atom (Figure 5). In peroxidases, the channel is not as constricted, and the peroxidatic substrate benzhydroxamic acid²⁶ binds to HRP in what is the equivalent of the constricted region of BpKatG closer to the heme. Substrate hydrogen peroxide entering the distal side cavity of BpKatG through the constricted portion of the channel would immediately come into contact with the active-site residues Arg109, Trp111 and His112 (Figure 5(b)) for generation of compound I in both the catalatic and peroxidatic modes of reaction, or for reduction of compound I in the catalatic reaction. Indeed, a continuum of water molecules is evident in this channel (Figure 5(b)). The mechanism by which organic substrates serve as electron donors for the peroxidatic reduction of compound I remains poorly defined.

Most peroxidases have a second access route, approximately in the plane of the heme, leading to the distal heme cavity, but the equivalent route in BpKatG is blocked by loops in the larger protein.

 $²F_{\rm o}-F_{\rm c}$ electron density map of the water molecules in the channel (modeled at 1σ in blue) and the $F_{\rm o}-F_{\rm c}$ electron density map showing the region of undefined density (modeled at 3σ in red) are shown. The interaction between the side-chain of Ser324 and the heme propionate group is indicated by the broken line. The surface feature map indicated in green was generated in the program VOIDOO.

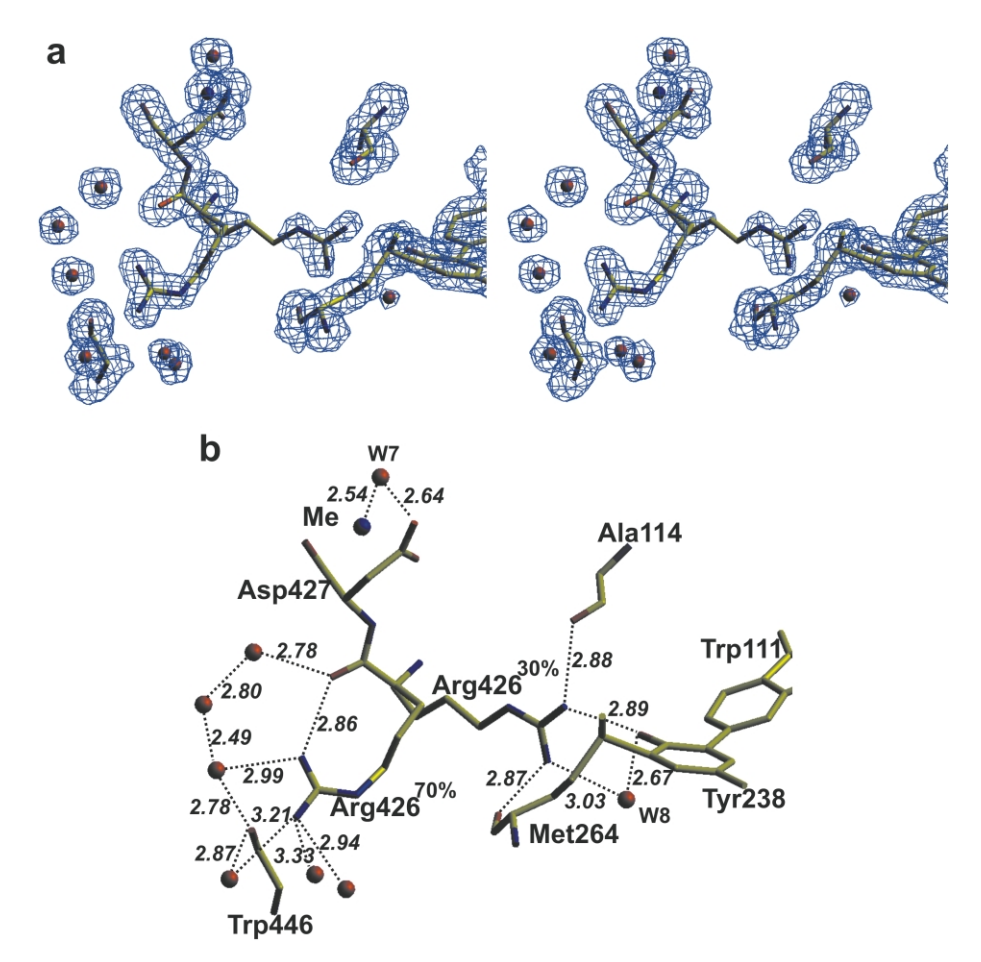


Figure 7. (a) Stereo view of the $2F_o - F_c$ electron density map modeled at 1σ in the vicinity of Arg426 with the model for both partial orientations of the Arg426 side-chain shown. The approximate proportions of the two orientations are indicated by the 30% and 70% designations. The main-chain atoms of Trp446 and other residues interacting with the Arg426 are included. (b) Model of the residues in the environment of Arg426 with the interactions indicated by broken lines and associated distances between atoms indicated in italics.

However, there does appear to be at least one other access channel providing direct access to the core of the protein in the vicinity of the single cation and to a region that encompasses two other structural features with possible functional significance. The first is a dramatic cleft in the side of the subunit formed between the two domains of the subunit that wraps around the protein. At one end of the cleft is located a well-defined, U-shaped region lined with polar residues (Figure 5(a)). Anionic residues, including the side-chains of Glu270, Asp587 and Glu589, and the carbonyl oxygen atoms of Ala262 and Ser265 surround a localized pocket of cationic groups including the side-chains of Lys422, Arg426 and Arg497. Significantly, the side-chains of Arg426 and Thr119 in their predominant conformations are located on the surface at the bottom of the U. They reduce the depth of the cleft slightly and allow the Arg426 side-chain to contribute to the cationic center on an otherwise predominantly anionic surface. Movement of the Arg426 side-chain to its minor conformation would increase the depth of the cleft and reduce the positively charged component on the surface. The associated rotation of the Thr119 side-chain would change the hydrogen bonding environment of the cleft by moving the side-chain OH group to a more external location. Such a striking and well-defined cavity, combined with the potential for functional changes through the simple movement of two side-chains, begs the suggestion that this is the binding site for a substrate. Unfortunately, the identity of the *in vivo* peroxidatic substrate of BpKatG remains unknown, but, if the cleft is a binding site, its elongated nature may imply a substrate with an extended, possibly even polymeric character.

A necessary extension of this model is that if a substrate did bind at this site, it would be necessary to transfer electrons from it to the heme for the reduction of compound I or II, as part of the peroxidatic reaction. A relatively short path for such electron tunneling is immediately obvious, beginning with the main-chain carbonyl group of Ala265 on the surface of the cleft adjacent to Met264. As part of the Met264-Tyr238-Trp111 adduct, the MetS is most likely carrying a positive charge and would provide a draw for electrons from the cleft. In turn, the adduct provides a direct pathway for electron transfer to the heme. Analysis

Table 2. Explanation of the phenotype of some mutations in KatG of M. tuberculosis on the basis of their location in the BpKatG structure

Mutation	Peroxidatic activity ^a	Residue	Effect of mutation in BpKatG
A. Category	1: mutations aff	ecting the II	NH reaction specifically
Ser315Thr	0.6	Ser324	Either the hydrogen bond with the propionate group of the heme is broken or significant dis- tortion in the side-chain is required to maintain hydrogen bonding and this would change the binding site for the hydrazine group of INH.
B. Category 2	2: mutations aff	ecting perox	idatic activity generally
Asn138Ser Leu148Arg	0.1	Asn142 Leu152	Binds to imidazole group of active-site His112 and change may distort spatial organization of active-site residues. Introduction of charged
Zeurionig	0.1	Ecuroz	guanidinium group into a polar region would require significant distor- tion of the main chain of the protein.
His270Gln	0.1	His279	The proximal side fifth ligand of the heme iron is removed, reducing heme binding
Thr275Pro	0.3	Thr284	Significant distortion in the main chain of the protein on the proximal side of the heme would be required to accommo-
Trp321Gly	0.3	Trp330	date the change. The indole ring is in close proximity to the proximal side His and removal may result in distortion of the mainchain atoms reducing heme binding and activity.
Asp381Gly	0.0	Asp389	activity. The aspartate side-chain interacts with the proximal side fifth ligand of the heme and its removal causes disruption in heme binding.
C. Group 3:	mutations with	an uncertaii	n mechanism
Leu587Pro	NDb	Leu594	The location is on the surface but far removed from the active site or INH binding site. Protein folding or stability may be affected

^a Selected MtKatG variants and their peroxidatic activities taken from Rouse et al.2

of the cleft may eventually provide insight into the in vivo substrate for KatG proteins.

In its minor conformation, the Arg426 side-chain is associated with the phenolic group on Tyr238 (Figure 7), similar to the predominant situation in

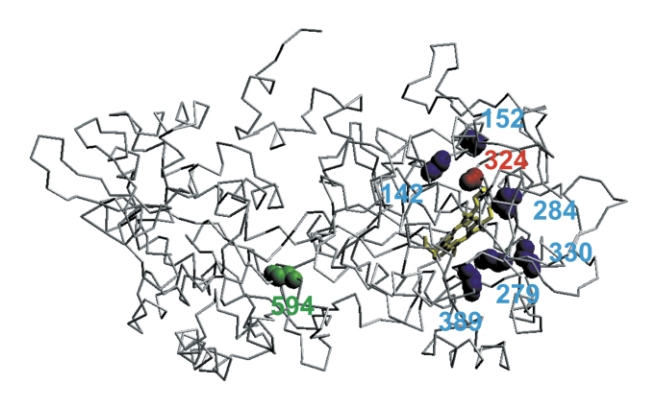


Figure 8. Location of mutations described in Table 2 located on a single subunit of BpKatG presented in the same orientation as the lower subunit shown in Figure 1(a). Only the main-chain atoms of the residues are shown and are represented as spheres. The residue in category 1 is colored red; the residues in category 2 are colored blue; and the residue in category 3 is colored green.

HmCP, where the Arg409 side-chain is associated with Tyr218. The cavity created by the movement of the side-chain to its predominant (>70%) conformation is located very close to the cleft region, and the slight movement of one or two side-chains would provide access from the cleft to the cavity. Perhaps more importantly, the other end of the cavity approaches the cation, which has direct access to the exterior through the second funnelshaped channel (Figure 5(a)). A region of electron density that cannot be explained by partial occupancy of the Arg426 side-chain is present in the cavity, suggesting the presence of another bound molecule. It is not clear if this is an alternate substrate-binding site, but the cavity would provide easy access for hydrogen peroxide needed for the oxidation of Met264 in the formation of the covalent linkage.

Analysis of the potential isoniazid binding site

A region of undefined electron density is located just before the constricted region in the main channel leading to the distal heme cavity of BpKatG (Figures 3 and 5). The location of the density is over 10 Å further away from the heme than is the benzhydroxamic acid bound in HRP, but is in close proximity to Ser324, the equivalent of Ser315 in MtKatG, which is thought to be involved in INH binding because changing it interferes with INH activation. This extra density was found both in the structure obtained after a short soaking with INH and in the structure obtained without soaking (Table 1). However, no INH had been introduced to the enzyme subsequent to purification, and only phosphate buffer was used during the purification, making exposure to other pyridine-like molecules unlikely. Therefore, it is concluded that the undefined density is the result of a metabolic constituent of E. coli, that may closely resemble INH. One such molecule is pyridoxol

ND-not determined.

or vitamin B6, a common growth-medium component, and its oxidation would lead to pyridoxal required for the synthesis of pyridoxal phosphate. Another closely related common metabolite is nicotinamide, although why it would require oxidation is not clear. The potential for involvement in modification of common metabolites provides a role for the catalase-peroxidases other than being simply protective enzymes removing hydrogen peroxide. More importantly, it provides an explanation for why the enzyme has a binding site for isoniazid, which is not a normal bacterial metabolite.

Definition of the binding of isoniazid is one of the main goals of elucidating the structure of KatG and, despite the distance from the heme, the region around Ser324 is a strong candidate for INH binding. To investigate this possibility further, models of INH and pyridoxol were superimposed into the region of undefined density, and the environment was analyzed for the likelihood of their binding (Figure 3). The surrounding region is composed predominantly of hydrophobic amino acid residues including Pro140, Ala143, Ala290, Val293, Trp309 and Ile322, all of which might interact with the region of density suggesting the presence of a relatively hydrophobic molecule. Only two potential ionic or hydrogen bonding opportunities are presented at opposite ends of the electron-dense region. The hydrogen bond of indole N of Trp309 with water molecule W5 could potentially interact with the N atom of the pyridine ring of INH, pyridoxol or nicotinamide. At the opposite end, the carbonyl oxygen atoms of Thr323 and Ser324 are situated such that an interaction with the hydrazine portion of INH is possible. The oxidizable -CH₂OH of pyridoxol would be oriented in close proximity to the same carbonyl oxygen atoms. The interaction of the nicotinamide -NH₂ group with the carbonyl group of Ile322 is predicted but the center to be oxidized is not evident, unless it is a very unusual reduced form of the ring.

The region in the main channel leading to the heme therefore presents a remarkably good candidate site for the binding of both INH and related pyridine derivatives. A possible mechanism for the oxidation of INH might involve distortion in the N-CO of INH bond caused by interaction with the Thr323-Ser324 carbonyl oxygen atoms. The side-chain of Ser324 forms a hydrogen bond with the carboxylate group of the heme propionate side-chain, and this direct association will result in a pull of electrons away from the serine residue towards the electron-deficient heme of compound I and compound II. This will result in polarization of the N-CO bond of INH, most likely leading to formation of the pyridine carbonyl and hydrazine radicals.²⁷ The pyridine carbonyl radical would be stabilized through resonance across the aromatic ring and delocalization of electrons from the pyridine nitrogen would break the hydrogen bond with water molecule W5, which might be necessary to allow reorientation of the molecule for

further reaction with NADH to form the InhA inhibitor.²⁸ The hydrazine radical might have an electron stripped for passage to the heme, generating a positively charged NH₂-NH⁺, which in turn would react rapidly with water to form NH2-NHOH. Speculatively, if a molecule such as pyridoxol is the substrate, it might bind, oriented similarly to what has been proposed for INH, resulting in the -CH₂OH para to the ring nitrogen atom being in close contact with the carbonyl oxygen atom of Thr322 ready for oxidation. As for INH, the electron-deficient heme of compounds I and II would serve to polarize electrons to promote the oxidation. Because Mn²⁺ was not introduced into the system and because KatG can activate INH independent of added Mn ion,²⁸ the role of Mn in this mechanism is not considered here.

This model provides an insight into the possible multiple roles of Ser315 of MtKatG in the oxidation of INH, and explains how its change to Thr would prevent reaction with INH. The first role lies in the main-chain interaction with the hydrazine portion of INH and direct participation in the catalytic reaction. The second role lies in providing a direct route for electron transfer from the INH to the radical of either compound I or compound II on the heme ring. Changing Ser to Thr would result in unfavorable interactions between the Thr sidechain and the heme propionate group in all conformers except one that could not form hydrogen bonds, thereby breaking the electron conduit. The other alternative of main-chain atom movement to allow hydrogen bonding would distort the catalytic site, preventing reaction.

All other residues in the pocket surrounding the INH-like electron density are fully conserved between BpKatG and MtKatG. Significantly, HMCP and the other catalase-peroxidases of haloarchaebacterial origin have a one residue insertion of Asp269 compared to BpKatG, located in a loop adjacent to the pocket. The insertion forces the ring of the adjacent Pro270 into a position that would interfere with the region of INH-like electron density. The implication is that HMCP should not bind INH in this region, and this might explain why a similar region of electron density was not observed in the HMCP electron density maps.

On the basis of the structure of BpKatG, the mechanisms by which the various clinically identified mutations in MtKatG^{1,29} may impart INH resistance can be divided into three categories (Table 2). The first category includes only the Ser315Thr variant (equivalent to Ser324 in BpKatG), which has a minor effect on peroxidatic activity but a significant effect on INH activation, suggesting that INH binding and/or transfer of electrons to the heme is affected. The second category includes six variants with reduced peroxidatic activities, and correspondingly reduced abilities to activate INH. Included are Asn138Ser, Leu148Arg, His270Gln, His275Pro, Trp321Gly and Asp381Gly (equivalent to Asn142, Leu152, His279, His284, Trp330 and Asp389, respectively, in

BpKatG). The third category contains only one variant, Leu587Pro (equivalent to Leu594), which seems to be impart INH-resistance through enzyme instability, most likely the result of defective folding. Other clinical isolates of MtKatG, initially thought to impart INH resistance, including Ser140Asn, Ala350Thr, Arg463Leu and Leu587-Met are not included in the Table, because the variants retain native peroxidatic activities and native abilities to activate INH.^{1,29} Also not included in the list are the active-site variants Arg104Leu and His108Gln, which directly modify catalytic residues. The locations of the residues in BpKatG equivalent to the residues included in Table 2 are shown in Figure 8. The single residue in the first category (colored red) is found in the channel leading to the heme; the six residues in the second category (colored blue) are found in the general vicinity of the heme; and the single residue in the third category (colored green) is in the C-terminal domain.

These comparisons are based on the presumption of extensive similarity between the *M. tuberculosis* and *B. pseudomallei* enzymes and, indeed, the two enzymes are very similar. The sequences are 64.6% identical over the complete sequence of 749 residues, and, more importantly, they are 75.7% identical over 272 residues (residues 88–359) in the catalytic core of the enzyme. The discussions are also based on the assumption that BpKatG utilizes isoniazid as a substrate, and radical generation by BpKatG is indeed at a rate equivalent to that of *E. coli* HPI, about one-fifth of that of MtKatG³⁰ (data not shown)

The design of derivatives of INH that would be more effective and might possibly curtail the developing widespread resistance to INH in different strains of *M. tuberculosis* was one hoped-for objective that would result from the definition of the structure of KatG. Unfortunately, the structure suggests that such a goal will be elusive. The variability in the INH-resistance phenotypes is a result of mutations spread widely throughout the enzyme with no single focus or mechanism. Furthermore, the structural environment of the potential INHbinding site does not present obvious motifs that might be exploited for the binding of INH derivatives. The binding site is composed largely of hydrophobic residues surrounding a relatively small volume that is apparently optimized for a pyridine ring with a limited number of substituents, including the carbonyl hydrazide group para to the pyridine nitrogen (Figure 3(b)). One note of optimism is the fact that other different pyridine derivatives seem to bind to the site.

Conclusions

The crystal structure of the catalase-peroxidase of *B. pseudomallei*, determined at 1.7 Å resolution, presents a number of structural features that can be interpreted as implying the existence of, as yet

undetermined, catalytic functions of the catalaseperoxidases. The immediate environment of the heme-containing active site is structurally similar to that of plant peroxidases and to the catalaseperoxidase from H. marismortui, confirming its already ascribed functions as a catalase and a peroxidase. Indeed, the potential binding site for isoniazid is found within what is considered to be the usual substrate access channel of peroxidases. Despite its binding to catalase-peroxidases and the interest this has generated, isoniazid is not a normal substrate for the enzyme, but analysis of its binding site, a small hydrophobic pocket with limited functional capability, suggests that the natural substrate cannot be too different in size or shape.

The presence of a modification on the heme, likely a perhydroxylation, of a single sodium ion in each subunit, of multiple conformations of sidechains and of a new access channel to a cavity in the subunit interior, all within the same region of the subunit, imply the existence of a second, functionally important part of the enzyme. Immediately adjacent to this region are a large cleft on the enzyme surface, suggestive of a binding site for an extended substrate, and the unusual adduct of the side-chains of Trp111, Tyr238 and Met264, presenting a possible route for electron tunneling to the heme from substrates bound either in the cavity or in the cleft on the surface. Further work is required to define the actual in vivo peroxidatic substrates of the catalase-peroxidases, and the structure of BpKatG will provide direction to that study.

Materials and Methods

Crystallization and structure determination

The BpKatG protein analyzed in this work was purified from the catalase-deficient E. coli strain UM262 as described.9 Crystals were obtained at 20 °C by the vapor-diffusion, hanging-drop method with 2 μl of a 22 mg/ml of protein solution and 1 µl of the reservoir solution containing 16-20% (w/v) polyethylene glycol (PEG 4K), 20% (v/v) 2-methyl-2,4-pentanediol (MPD) and 0.1 M sodium citrate pH 5.6.9 Diffraction data were obtained from crystals cooled with a nitrogen cryostream using the same reservoir solution as cryobuffer at 20% PEG-4K. However, the best data set was obtained from a crystal where 100 mM INH had been added to the cryobuffer (Table 1). Crystals were primitive orthorhombic space group $P2_12_12_1$ with one dimeric molecule in the crystal asymmetric unit. The diffraction data set was processed using the program DENZO and scaled with program SCALEPACK. 31 A part (10%) of the measured reflections in every data set were reserved for R_{free} monitoring during automatic refinement (Table 1). All the structural analysis reported in this work, except where indicated explicitly, has been done on the structure derived from the crystals soaked briefly with INH. However, no significant differences have been found with respect to the structure obtained without being exposed to INH. Even the extra density found in the major channel leading to the heme is found in both structures. Therefore, the structure derived from the crystal

after a short soak in INH is considered to be the native BKG structure. Reference to the unsoaked data set has been added only as a control to the presence of INH.

Structure determination was carried out with the program AMoRe³² and the CPx of H. marismortu⁵ as searching model. Phases were improved and extended to 1.7 Å resolution with the program ARP-WARP.³³ The resulting map showed clear continuity over the complete length of BpKatG from Asn35 to Ala748 in both subunits. The quality of the data was confirmed by the clarity in the electron density of a number of errors in a 12 amino acid residue region of the predicted sequence. Refinement was started with programs in the CNS suite³⁴ and completed using the program REFMAC35 with solvent molecules modeled with the program WATPEAK36 and manually with the graphics program O.37 Solvent molecules were introduced only when they corresponded to the strongest peaks in the difference Fourier maps that could make at least one hydrogen bond with atoms already in the model. In the final rounds of refinement, the two subunits were treated independently with the bulk solvent correction applied and the whole resolution range available used for each variant (Table 1). The analysis of solvent accessibility and molecular cavities was carried out with program VOIDOO38 using a reduced atomic radius for polar atoms in accounting for possible hydrogen bonds.³⁹ All the Figures were prepared using SETOR.40

Protein Data Bank accession number

Structure factors and coordinates have been submitted to the Protein Data Bank under accession number 1MWV.

Acknowledgements

This work was supported by grants from DGICYT (BIO099-0865 and BIO2002-04419) to I.F., and OGP9600 from the Natural Sciences and Engineering Research Council of Canada (NSERC) to P.C.L. Many thanks are due to R. Perez and R. Eritja for their help in the experimental work.

References

- 1. Heym, B., Alzari, P. M. & Honoré, N. and Cole, S. T. (1995). Missense mutations in the catalase-peroxidase gene, *katG* are associated with isoniazid resistance in *Mycobacterium tuberculosis*. *Mol. Microbiol.* **15**, 235–245.
- 2. Hillar, A., Peters, B., Pauls, R., Loboda, A., Zhang, H., Mauk, A. G. & Loewen, P. C. (2000). Modulation of the activities of catalase-peroxidase HPI of *Escherichia coli* by site directed mutagenesis. *Biochemistry*, **39**, 5868–5875.
- 3. Regelsberger, G., Jakopitsch, C., Ruker, F., Krois, D., Peschek, G. A. & Obinger, C. (2000). Effect of distal cavity mutations on the formation of compound I in catalase-peroxidases. *J. Biol. Chem.* 275, 22854–22861.
- 4. Regelsberger, G., Jakopitsch, C., Furtmuller, P. G., Rueker, F., Switala, J., Loewen, P. C. & Obinger, C. (2001). The role of distal tryptophan in the bifunc-

- tional activity of catlase-peroxidases. *Biochem. Soc. Trans.* **29**, 99–105.
- 5. Yamada, Y., Fujiwara, T., Sato, T., Igarashi, N. & Tanaka, N. (2002). The 2.0 Å crystal structure of catalase-peroxidase from *Haloarcula marismortui*. *Nature Struct. Biol.* **9**, 691–695.
- Zhang, Y., Heym, B., Allen, B., Young, D. & Cole, S. (1992). The catalase-peroxidase gene and isoniazid resistance of *Mycobacterium tuberculosis*. *Nature*, 358, 591–593.
- 7. Yamada, Y., Saijo, S., Sato, T., Igarashi, N., Usui, H., Fujiwara, T. & Tanaka, N. (2001). Crystallization and preliminary X-ray analysis of catalase-peroxidase from the halophilic archaeon *Haloarcula marismortui*. *Acta Crystallog. sect. D*, **57**, 1157–1158.
- 8. Wada, K., Tada, T., Nakamura, Y., Kinoshita, T., Tamoi, M., Sigeoka, S. & Nishimura, K. (2002). Crystallization and preliminary X-ray diffraction studies of catalase-peroxidase from Synechococcus PCC7492. *Acta Crystallog. sect. D*, **58**, 157–159.
- 9. Carpena, X., Switala, J., Loprasert, S., Mongkolsuk, S., Fita, I. & Loewen, P. C. (2002). Crystallization and preliminary X-ray analysis of the catalase-peroxidase KatG from *Burkholderia pseudomallei*. *Acta Crystallog*. sect. D, 58, 2184–2186.
- Carpena, X., Guarne, A., Ferrer, J. C., Alzari, P. M., Fita, I. & Loewen, P. C. (2002). Crystallization and preliminary X-ray analysis of the hydroperoxidase I C-terminal domain from *Escherichia coli*. Acta Crystallog. sect. D, 58, 853–855.
- 11. Welinder, K. G. (1991). Bacterial catalase-peroxidases are gene duplicated members of the plant peroxidase superfamily. *Biochim. Biophys. Acta*, **1080**, 215–220.
- 12. Claiborne, A. & Fridovich, I. (1979). Purification of the *o*-dianisidine peroxidase from *Escherichia coli* B. Physicochemical characterization and analysis of its dual catalatic and peroxidatic activities. *J. Biol. Chem.* **254**, 4245–4252.
- 13. Wilming, M. & Johnsson, K. (2001). Inter- and intramolecular domain interactions of the catalase-peroxidase KatG from *M. tuberculosis*. *FEBS Letters*, **509**, 272–276.
- Laskowski, R. A., MacArthur, M. W., Moss, D. S. & Thornton, J. M. (1993). PROCHECK: a program to check the stereochemical quality of protein structures. J. Appl. Crystallog. 26, 283–291.
- tures. *J. Appl. Crystallog.* **26**, 283–291.

 15. Weik, M., Ravelli, R. B. G., Kryger, G., McSweeney, S., Raves, M. L., Harel, M. *et al.* (2000). Specific chemical and structural damage to proteins produced by synchrotron radiation. *Proc. Natl Acad. Sci USA*, **97**, 623–628.
- 16. Ravelli, R. B. G. & McSweeney, S. M. (2000). The fingerprint that X-rays can leave on structures. *Structure*, **8**, 315–328.
- 17. Chouchane, S., Lippai, I. & Magliozzo, R. S. (2000). Catalase-peroxidase (*Mycobacterium tuberculosis* KatG) catalysis and isoniazid activation. *Biochemistry*, **39**, 9975–9983.
- 18. Creighton, T. E. (1993). *Proteins: Structures and Molecular Properties*, 2nd edit., Freeman, New York.
- Choinowski, T., Blodig, W., Winterhalter, K. H. & Piontek, K. (1999). The crystal structure of lignin peroxidase at 1.70 Å resolution reveals a hydroxy group on the C^β of tryptophan 171: a novel radical site formed during the redox cycle. *J. Mol. Biol.* 286, 809–827.
- Henriksen, A., Welinder, K. G. & Gajhede, M. (1998). Structure of barley grain peroxidase refined at 1.9 Å resolution. J. Biol. Chem. 273, 2241–2248.

- Naruse, N., Oka, M., Konishi, M. & Oki, T. (1993).
 New antiviral antibiotics, kistamicins A and B. II.
 Structure determination. J. Antibiot. 46, 1812–1818.
- 22. Elder, A. M. & Rich, D. H. (1999). Two syntheses of the 16- and 17-membered DEF ring systems of chloropeptin and complestatin. *Org. Letters*, **1**, 1443–1446.
- 23. Buzy, A., Bracchi, V., Sterjiades, R., Chroboczek, J., Thibault, P., Gagon, J. *et al.* (1995). Complete amino acid sequence of *Proteus mirabilis* PR catalase. Occurrence of a methionine sulfone in the close proximity of the active site. *J. Protein Chem.* **14**, 59–72.
- Murshudov, G. N., Grebenko, A. I., Barynin, V., Dauter, Z., Wilson, K., Vainshtein, B. K. et al. (1996).
 Structure of the heme d of *Penecillium vitale* and *Escherichia coli* catalases. J. Biol. Chem. 271, 8863–8868.
- 25. Bravo, J., Fita, I., Ferrer, J. C., Ens, W., Hillar, A., Switala, J. & Loewen, P. C. (1997). Identification of a novel bond between a histidine and the essential tyrosine in catalase HPII of *Escherichia coli*. *Protein Sci.* **6**, 1016–1023.
- Henriksen, A., Schuller, D. J., Meno, K., Welinder, K. G., Smith, A. T. & Gajhede, M. (1998). Structural interactions between horseradish peroxidase C and the substrate benzhydroxamic acid determined by X-ray crystallography. *Biochemistry*, 37, 8054–8060.
- Rozawarski, D. A., Grant, G. A., Barton, D. H. R., Jacobs, W. R., Jr & Sacchettini, J. C. (1998). Modification of the NADH of the isoniazid target (INHA) from Mycobacterium tuberculosis. Science, 279, 98–102.
- Lei, B., Wei, C. J. & Tu, S. C. (2000). Activation mechanism of antitubercular isoniazid: activation by *Mycobacterium tuberculosis* KatG, isolation and characterization of InhA inhibitor. *J. Biol. Chem.* 275, 2520–2526.
- Rouse, D. A., DeVito, J. A., Li, Z., Byer, H. & Morris, S. L. (1996). Sute-directed mutagenesis of the *katG* gene of *Mycobacterium tuberculosis*: effects on catalaseperoxidase activities and isoniazid resistance. *Mol. Microbiol.* 22, 583–592.

- Hillar, A. & Loewen, P. C. (1995). Comparison of isoniazid oxidation catalyzed by bacterial catalase-peroxidase and horseradish peroxidase. *Arch. Biochem. Biophys.* 323, 438–446.
- 31. Otwinowski, Z. & Minor, W. (1996). Processing of X-ray diffraction data collected in oscillation mode. *Methods Enzymol.* **276**, 307–326.
- 32. Navaza, J. (1994). AMoRe: an automated package for molecular replacement. *Acta Crystallog. sect. A*, **50**, 157–163.
- 33. Lamzin, V. S. & Wilson, K. S. (1997). Automated refinement for protein crystallography. *Methods Enzymol.* **277**, 269–305.
- Brünger, A. T., Adams, P. D., Clore, G. M., DeLano, W. L., Gros, P., Grosse-Kunstleve, R. W. et al. (1998).
 Crystallography and NMR system (CNS): a new software suite for macromolecular structure determination. Acta Crystallog. sect. D, 54, 905–921.
- 35. Murshudov, G. N., Vagin, A. A. & Dodson, E. J. (1997). Refinement of macromolecular structures by the maximum-likelihood method. *Acta Crystallog. sect. D*, **53**, 240–255.
- Collaborative Computational Project, Number 4 (1994). The CCP4 suite: programs for protein crystallography. Acta Crystallog. sect. A, 50, 760–763.
- 37. Jones, T. A., Zou, J. Y., Cowan, S. W. & Kjeldgaard, M. (1991). Improved methods for building protein models in electron density maps. *Acta Crystallog. sect. A*, **47**, 110–119.
- 38. Kleywegt, G. J. & Jones, T. A. (1994). Detection, delineation, measurement and display of cavities in macromolecule structures. *Acta Crystallog. sect. D*, **50**, 178–185.
- Maté, M. J., Sevinc, M. S., Hu, B., Bujons, J., Bravo, J., Switala, J. et al. (1999). Mutants that later the covalent structure of catalase hydroperoxidase II from Escherichia coli. J. Biol. Chem. 274, 27717–27725.
- 40. Evans, S. (1993). SETOR: hardware lighted three-dimensional solid model representations of macromolecules. *J. Mol. Graph.* **11**, 134–138.

Edited by R. Huber

(Received 24 October 2002; received in revised form 6 January 2003; accepted 17 January 2003)



FEMS Microbiology Letters 225 (2003) 167-172



www.fems-microbiology.org

Oxidant-inducible resistance to hydrogen peroxide killing in Agrobacterium tumefaciens requires the global peroxide sensor-regulator OxyR and KatA

Warawan Eiamphungporn ^a, Kaewkanya Nakjarung ^a, Benjaphorn Prapagdee ^b, Paiboon Vattanaviboon ^{c,*}, Skorn Mongkolsuk ^{a,c,**}

- ^a Department of Biotechnology, Faculty of Science, Mahidol University, Bangkok 10400, Thailand
- ^b Post-graduate Education, Training and Research Program in Environmental Science, Technology and Management, Asian Institute of Technology, Pathumthani 12120, Thailand
 - ^c Laboratory of Biotechnology, Chulabhorn Research Institute, Lak Si, Bangkok 10210, Thailand

Received 30 April 2003; received in revised form 18 June 2003; accepted 24 June 2003

First published online 16 July 2003

Abstract

Induced adaptive and cross-protective responses to peroxide stress are important strategies used by bacteria to survive stressful environments. We have shown that exposure to low levels of peroxide (adaptive) and superoxide anions (cross-protection) induced high levels of resistance to peroxide killing in Agrobacterium tumefaciens. The mechanisms and genes involved in these processes have not been identified. Here, the roles played by peroxide (oxyR) and superoxide (soxR) global regulators and a catalase gene (katA) during these responses were investigated. H_2O_2 -induced adaptive protection was completely abolished in both the oxyR and katA mutants. Superoxide generator (menadione)-induced cross-protection to H_2O_2 killing was observed in a soxR mutant, but not in either an oxyR or a katA mutant. In vivo analysis of the katA promoter, using a katA::lacZ transcriptional fusion, revealed that it could be induced by menadione in an oxyR-dependent manner. These results lead us to conclude that H_2O_2 and superoxide anions directly or indirectly oxidize OxyR and it is the resulting activation of katA expression that is responsible for the induced protection against lethal concentrations of H_2O_2 . © 2003 Federation of European Microbiological Societies. Published by Elsevier Science B.V. All rights reserved.

Keywords: Agrobacterium tumefaciens; Adaptation; Catalase; H2O2; Menadione; oxyR; soxR

1. Introduction

Agrobacterium tumefaciens is a plant pathogenic soil bacterium that infects wound sites in many dicotyledonous plants causing the formation of crown gall tumors through the insertion of a segment (T-DNA) of the tumor-inducing (Ti) plasmid into the nucleus of the infected cells [1]. This microorganism is also widely used for the introduction of foreign genes into plant cells and the generation of genetically engineered plants [2].

Fax: +66 (2) 574 2027.

Fax: +66 (2) 574 2027.

E-mail addresses: paiboon@tubtim.cri.or.th (P. Vattanaviboon), skorn@tubtim.cri.or.th (S. Mongkolsuk).

Aerobically growing bacteria always encounter reactive oxygen species (ROS) that are generated as by-products of oxygen-dependent metabolism [3]. In addition, rapid production and accumulation of ROS is an important part of the initial plant defense response against invading microorganisms [4]. ROS are highly toxic to bacterial cells and bacteria have evolved several enzymatic and non-enzymatic mechanisms to protect themselves against them. Physiological adaptation to is one of the important protective strategies used by bacteria when growing under oxidative stress conditions [5–9]. Exposure to sublethal concentrations of one oxidant can induce a protective response against subsequent exposure to lethal concentrations of either the same oxidant (adaptive protection) or unrelated agents (cross-protection) [5]. Oxidant-induced protective responses often result from the coordinated activation of gene(s) involved in both oxidant detoxification and damage repair [10]. Intensive studies, done in the en-

^{*} Corresponding author. Tel.: +66 (2) 574 0630;

^{**} Corresponding author. Tel.: +66 (2) 574 0622 ext. 3816;

teric bacterium *Escherichia coli*, show that key regulators of the adaptive response in this organism are the oxidant sensing transcriptional regulators SoxRS and OxyR, which regulate the inducible expression of antioxidant genes in response to superoxide anion and H₂O₂ exposure, respectively [11].

We have demonstrated the existence of H_2O_2 -induced adaptive and menadione-induced cross-protection against H_2O_2 killing treatments in *A. tumefaciens* [12]. These inducible responses could play important roles in plant/microbe interactions since the initial active plant defense against microbes involves the increased production and accumulation of H_2O_2 and other ROS [4]. Here we report the characterization of the regulatory and structural gene responsible for these responses.

2. Materials and methods

2.1. Bacterial growth conditions

A. tumefaciens NTL4 [13] and mutant strains were grown aerobically in LB medium at 30°C with continuous shaking at 150 rpm. Overnight cultures were inoculated into fresh LB medium to give an OD_{600} of about 0.1. Exponential phase $(OD_{600}$ about 0.6, after 4 h of growth) cells were used in all experiments, as indicated.

2.2. Molecular biology techniques

General molecular genetics techniques including plasmid preparation, restriction endonuclease digestion, ligation, transformation in *E. coli* and agarose electrophoresis were performed using standard protocols [14]. Plasmid purification for DNA sequencing was performed using a Qiaprep Spin Miniprep kit (Qiagen). DNA was sequenced using a BigDye terminator cycle sequencing kit (PE Biosystems) on an ABI 310 automated DNA sequencer (Applied Biosystems Inc.). *A. tumefaciens* was transformed by electroporation under conditions previously described [13].

2.3. Construction of a soxR mutant

Two primers designed from the putative *A. tumefaciens* soxR nucleotide sequence (AE009322), BT523-5'TGA-TACGCGTCTGGAGC 3' and BT524-5'TCGAAGGC-TGGCGCACC 3', were used to amplify a 210-bp soxR fragment from *A. tumefaciens* NTL4 genomic DNA using the polymerase chain reaction (PCR). The PCR product was cloned into pGEM-T-easy (Promega) before determining its nucleotide sequence. Subsequently, a SaII-SacII fragment of the PCR clone was subcloned into pKNOCK-Gm [15], a non-replicative plasmid in *Agrobacterium*, cut with the same restriction enzymes. The resultant plasmid, pKNOCKsoxR, was then transferred to *A. tumefaciens* by conjugation. A soxR mutant was generated by a homolo-

gous recombination of the *soxR* fragment in pKNOCK-soxR and its counterpart on the NTL4 chromosome. Inactivation of *soxR* was confirmed by PCR using two specific primers: one located upstream of the insertion site and the other located on the pKNOCK-Gm vector sequence.

2.4. Determination of resistance levels to oxidants

The peroxide-induced adaptive and cross-protective experiments were performed by adding either 250 μ M H₂O₂ or 200 μ M menadione to exponential phase cultures. These cultures were grown for an additional 30 min before aliquots of cells were removed and treated with a range of lethal concentrations of H₂O₂ (20, 30, 40 mM) for 30 min. After treatment, cells were removed and washed once with fresh LB before appropriate dilutions were plated on LB agar. Colonies were counted after 48 h incubation at 30°C. Surviving fractions were defined as the number of colony forming units (cfu) recovered after the treatment divided by the cfu prior to treatment. All experiments were independently repeated three times and representative data are shown.

2.5. Superoxide dismutase (SOD) activity gels and assays

Xanthine–xanthine oxidase coupled reduction of cytochrome *c* was used to monitor total SOD activity [16]. One unit of SOD activity was defined as the amount of enzyme required to inhibit the rate of reduction of cytochrome *c* by 50%. To visualize SOD activity, non-denaturing electrophoresis was performed using a 10% polyacrylamide gel (pH 8.7) with a 5% stacking gel (pH 8.0) followed by staining with nitroblue tetrazolium/riboflavin photochemical stain as described by Beauchamp and Fridovich [17]. In the enzyme inhibition tests H₂O₂ or potassium cyanide were added to a riboflavin-TEMED solution at final concentrations of 5 and 2 mM, respectively. [Cu,Zn]-SOD is inactivated by cyanide and [Fe]-SOD by H₂O₂ while [Mn]-SOD is resistant to both.

3. Results and discussion

3.1. Induced adaptive protection against H₂O₂ killing requires functional oxyR and katA

In *A. tumefaciens*, exposure to sublethal concentrations of H_2O_2 is known to induce adaptive protection to a subsequent treatment with lethal concentrations of H_2O_2 (Fig. 1A) [12]. The regulatory gene involved in this process has not been identified. Thus, the role of OxyR, a global regulator of the peroxide stress response, in the process was investigated using the *oxyR* mutant strain PN03 [18]. PN03 was grown to exponential phase prior to pretreatment with 200 μ M H_2O_2 for 30 min. The induced cultures

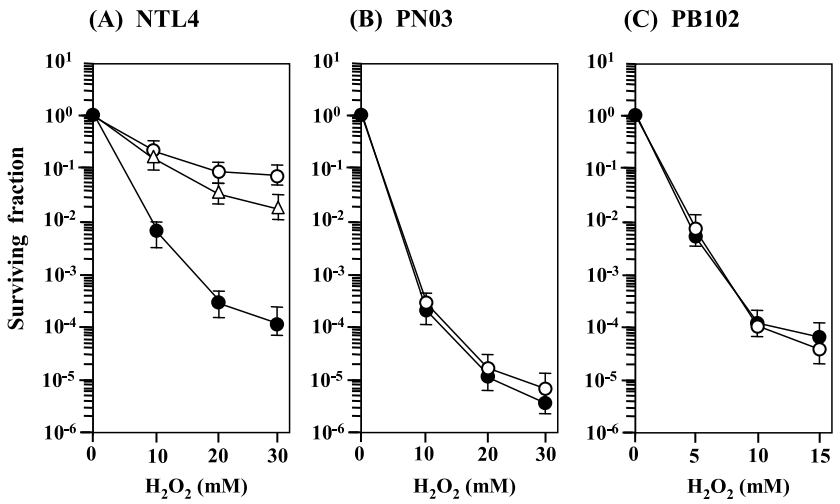


Fig. 1. Induced adaptive responses to H_2O_2 in various A. tumefaciens strains. The induced protection experiments were performed by adding 250 μ M H_2O_2 to exponential phase cultures of A. tumefaciens NTL4 (A), PN03 (B), and PB102 (C). These cultures were grown for an additional 30 min before aliquots of cells were removed and treated with the indicated concentrations of H_2O_2 for 30 min. After treatment, cells were removed and washed once with fresh LB before appropriate dilutions were plated on LB agar. Colonies were counted after 48 h incubation at 30°C. Surviving fractions were defined as cfu recovered after the treatment divided by cfu prior to treatment. All experiments were independently repeated three times and representative data are shown. (\bullet), uninduced; (\bigcirc), H_2O_2 -induced; and (\triangle), menadione-induced (cultures were induced with 200 μ M menadione).

were subsequently treated with lethal concentrations of H_2O_2 for 30 min. The results clearly showed that H_2O_2 -induced adaptation, against subsequent killing by the oxidant, was completely abolished in PN03 (Fig. 1B) indicating that functional OxyR was required for the response. Similar observations regarding the essential role of OxyR in peroxide adaptive responses have been made in *E. coli* and *Xanthomonas campestris* [19–21]. The data suggest that the adaptive response is due to the oxidation of OxyR during the peroxide pretreatment that leads to upregulation of the genes in the OxyR regulon. Thus, we extended the investigation to determine which genes in the OxyR regulon are required for the increased resistance

to H_2O_2 . We have previously shown that the expression of katA, encoding a bifunctional catalase–peroxidase HPI, could be induced by pretreatment of A. tumefaciens with sublethal concentrations of H_2O_2 in an OxyR-dependent manner [18]. In many bacteria, catalase levels correlate with the levels of H_2O_2 resistance [5,6,9]. Consequently, the role of katA in the H_2O_2 adaptive response was investigated using an A. $tumefaciens\ katA$ mutant (PB102). The results show that inactivation of katA abolished the adaptive response (Fig. 1C). Although, there are many genes that are regulated by OxyR, the results suggest that upregulation of katA alone is sufficient to confer protection against H_2O_2 killing in A. tumefaciens.

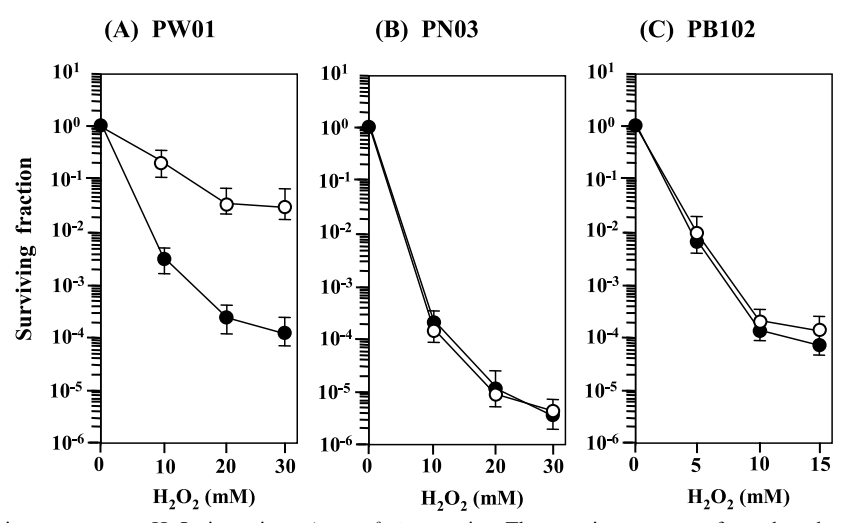
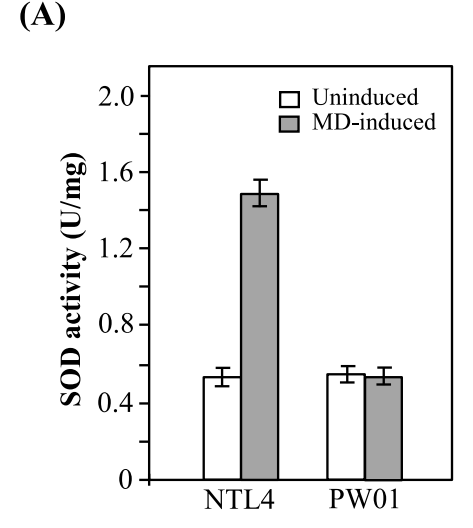


Fig. 2. Induced cross-protective responses to H_2O_2 in various A. tumefaciens strains. The experiment was performed as described in the legend to Fig. 1 except 200 μ M menadione was used for the induction instead of 250 μ M H_2O_2 . A. tumefaciens PW01 (A), PN03 (B) and PB102 (C) were used in the experiments. (\bullet), uninduced; (\bigcirc), menadione-induced.



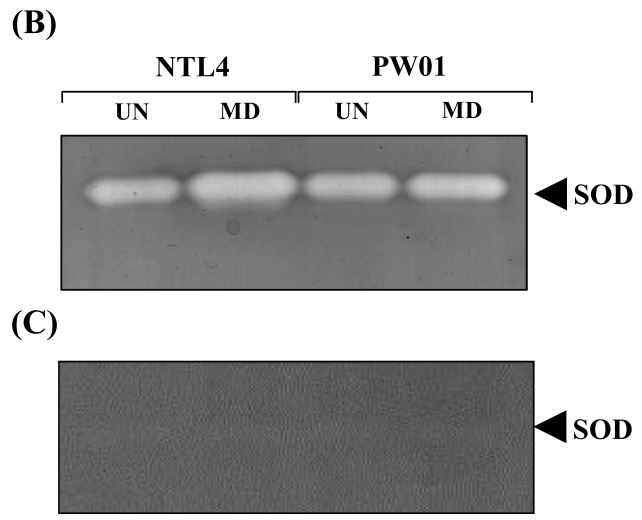


Fig. 3. Induction of SOD by menadione pretreatment in A. tumefaciens. A: Total SOD activity in cleared lysates prepared from exponential phase cultures of A. tumefaciens NTL4 and PW01 grown under uninduced and menadione (200 μ M)-induced conditions. B: SOD activity stain of cleared lysates (50 μ g total protein) of uninduced (UN) and menadione-induced (MD) cultures of NTL4 and PW01 separated on a non-denaturing polyacrylamide gel. SOD activity staining was performed as described in Section 2. C: SOD activity stain of a non-denaturing polyacrylamide gel, identical to that described in (B) that was treated with H_2O_2 prior to staining.

3.2. Menadione-induced cross-protection against H_2O_2 killing is soxR-independent

Treatment of *A. tumefaciens* NTL4 with 200 μM of the superoxide generator, menadione, induced cross-protection to a subsequent challenge with lethal concentrations of H₂O₂ (Fig. 1A) [12]. In *E. coli*, superoxide anions mediate changes in global gene expression via the superoxide sensing transcriptional regulators SoxR and SoxS [11,22]. Analysis of the *A. tumefaciens* genome [23] using the BLASTP program [24] revealed the presence of an open reading frame (ORF) (Atu3915) that encodes a 151-ami-

no-acid polypeptide with 55% sequence identity to E. coli SoxR. The A. tumefaciens SoxR homolog also contains a conserved CX2CXCX5C domain that is involved in the formation of the Fe-S cluster (data not shown). We inactivated the gene resulting in the A. tumefaciens soxR mutant strain designated PW01. PW01 was used to determine the role of SoxR in the menadione-induced cross-protection to H_2O_2 . The results in Fig. 2A clearly show that the ability of menadione treatment to induce cross-protection against subsequent exposure to H₂O₂ was retained in PW01, indicating that soxR was not responsible for mediating the response. The ability of menadione pretreatment to induce the elevated expression of genes in the soxRregulon was also tested by measuring SOD activity in cleared lysates prepared from cultures of strains NTL4 and PW01 grown under uninduced and menadione (200 µM)-induced conditions. The results clearly showed that pretreatment of NTL4 with menadione resulted in a 2.7-fold increase in total SOD activity and this induction was abolished in the soxR mutant PW01 (Fig. 3A). This evidence suggested that induction of genes in the soxRS regulon was not sufficient to protect A. tumefaciens from H_2O_2 toxicity.

Analysis of the genome also revealed that A. tumefaciens possesses three putative ORFs (namely Atu0876, Atu4583 and Atu4762) identified as SODs and all of these ORFs show a high degree of homology to the family of [Mn,Fe]-SOD [23]. However, only one band of SOD activity was observed by activity staining of polyacrylamide gels of lysates of A. tumefaciens NTL4 and PW01 grown under both uninduced and menadione-induced conditions (Fig. 3B). In order to distinguish which family of SOD isozymes was responsible for the activity detected in the gels, the experiments were repeated and the gels were soaked in either H₂O₂ or potassium cyanide prior to SOD activity staining. The results revealed that the inducible SOD band could be detected in the cyanide-treated gel (data not shown) but not in the H₂O₂-treated gel (Fig. 3C), indicating that a [Fe]-SOD was responsible for the observed SOD activity. The gene encoding this SOD is currently being characterized.

3.3. Induction of katA promoter by menadione is mediated by OxyR

We have previously shown that catalase levels correlate with the resistance levels to H_2O_2 [12]. The possibility that menadione-induced cross-protection to H_2O_2 killing is a result of the OxyR-dependent induction of katA expression was investigated. In vivo promoter analysis using pP_{katA} containing the katA promoter region transcriptionally fused to a promoter-less lacZ (katA::lacZ) was performed in NTL4 and PN03. The levels of β -galactosidase activity in bacterial cultures were determined under menadione-induced and uninduced conditions. The β -galactosidase activity from NTL4 bearing pP_{katA} was increased